OPEN ACCESS



Investigating the Magnetic Structure of Interplanetary Coronal Mass Ejections Using Simultaneous Multispacecraft In Situ Measurements

F. Regnault , N. Al-Haddad , N. Lugaz , C. J. Farrugia , W. Yu , E. E. Davies , A. B. Galvin , and B. Zhuang

¹ Space Science Center, Institute for the Study of Earth, Oceans, and Space, University of New Hampshire, USA; florian.regnault@unh.edu

² Austrian Space Weather Office, GeoSphere Austria, Graz, Austria

**Response of 2003 New York (2003 New York) (2

Received 2022 November 28; revised 2023 July 14; accepted 2023 August 9; published 2023 October 26

Abstract

In situ measurements from spacecraft typically provide a time series at a single location through coronal mass ejections (CMEs), and they have been one of the main methods to investigate CMEs. The CME properties derived from these in situ measurements are affected by temporal changes that occur as the CME passes over the spacecraft, such as radial expansion and aging, as well as spatial variations within a CME. This study uses multispacecraft measurements of the same CME at close separations to investigate both the spatial variability (how different a CME profile is when probed by two spacecraft close to each other) and the so-called aging effect (the effect of the time evolution on in situ properties). We compile a database of 19 events from the past 4 decades measured by two spacecraft with a radial separation of <0.2 au and an angular separation of <10°. We find that the average magnetic field strength measured by the two spacecraft differs by 18% of the typical average value, which highlights nonnegligible spatial or temporal variations. For one particular event, measurements taken by the two spacecraft allow us to quantify and significantly reduce the aging effect to estimate the asymmetry of the magnetic field strength profile. This study reveals that single-spacecraft time series near 1 au can be strongly affected by aging and that correcting for self-similar expansion does not capture the whole aging effect.

Unified Astronomy Thesaurus concepts: Solar coronal mass ejections (310); Heliosphere (711)

1. Introduction

Magnetic instabilities occurring in the solar atmosphere can lead to the ejection of magnetic structures that subsequently propagate through the corona and heliosphere. Such events are referred to as coronal mass ejections (CMEs). They have been imaged in the corona by white-light coronagraphs since the early 1970s (Tousey 1973) and are now routinely imaged by the SOHO/LASCO (Brueckner et al. 1995) and STEREO/ SECCHI/COR1,2 (Howard et al. 2008) coronagraphs. In addition, in situ instruments on board interplanetary probes directly measure the magnetic and plasma properties of CMEs as they pass over the spacecraft. When measured in situ, CMEs are typically composed of a dense and hot sheath, preceded about half the time by a fast-forward shock (Jian et al. 2006; Salman et al. 2020a), and a low proton β , high magnetic field, low-temperature magnetic ejecta (ME; Salman et al. 2020a; Regnault et al. 2020). Based on such measurements of the same event by five spacecraft, Burlaga et al. (1981) identified magnetic clouds (MCs) as one type of ME that have clearly defined properties, i.e., a rotation of the magnetic field vector, strong magnetic field strength, and low proton temperature. However, more than half the events measured in situ at 1 au do not have these signatures (Gosling 1990; Richardson & Cane 2010). In this study, we use the term ME to denote the ejecta part of the CME, irrespective of whether or not it is an MC. Traditionally, there has been a distinction between CMEs observed remotely in the corona and interplanetary CMEs, or ICMEs, measured in situ by spacecraft. However, since the

Original content from this work may be used under the terms of the Creative Commons Attribution 4.0 licence. Any further distribution of this work must maintain attribution to the author(s) and the title of the work, journal citation and DOI.

2000s, it has been possible to remotely observe ICMEs in interplanetary space, first with SMEI (Eyles et al. 2003) and then STEREO/HI (Harrison et al. 2009); more recently, it has become possible to measure CMEs in situ in the upper corona and innermost heliosphere with the Parker Solar Probe and Solar Orbiter. Both of these missions combine in situ measurements and remote observations, often simultaneously, of CMEs/ICMEs. As such, the distinction between CMEs and ICMEs has become smeared and harder to justify. Throughout this paper, we use the term "CME" to describe the whole ejection, irrespective of how and where it is measured. In doing so, we follow the conventions of past researchers during the last decade (e.g., see Howard & DeForest 2012; Lugaz et al. 2015). This also follows decades of research that have clearly identified the CMEs measured in the corona as the source of the CMEs measured in situ (e.g., see Bothmer & Schwenn 1998).

Most of the time, in situ measurements of CMEs are from a single spacecraft. This provides the equivalent to a 1D cut through the 3D CME structure under the assumption of a CME being a static structure. The limitations of such measurements make it difficult to investigate the global properties of the 3D structure of CMEs. For this reason, fitting and reconstruction techniques, like the Grad-Shafranov technique (Hu & Sonnerup 2002) or the Lundquist analytical model (Lundquist 1951; Burlaga 1988; Lepping et al. 1990), have been developed to deduce the global properties of the CME using a singlespacecraft in situ time series. Such techniques, however, require strong assumptions, such as the presence of an invariance direction and/or assumptions on the shape of the magnetic structure, that are not always justified and typically cannot be tested. Most often, the ME structure is assumed to be that of a highly twisted magnetic flux rope, and even other types of structures may be reconstructed as such (Al-Haddad et al. 2011, 2019). In addition, different techniques are often found to be inconsistent with one another (Riley et al. 2004; Al-Haddad et al. 2013; Martinić et al. 2022). For this reason, in this study, we limit the number of assumptions that we make, staying away from fitting techniques, and try to interpret the data without relying on models as much as possible. Our main assumption in this study is that the ME is a coherent magnetic structure up to an angular separation of 15° – 20° (Owens et al. 2017; Lugaz et al. 2018). Moreover, we emphasize that we use the more general definition of ME throughout this study and therefore do not assume that the ME must have a magnetic flux rope structure or correspond to an MC being crossed away from its center. Thus, we do not assume that there is an invariant direction in the MEs we analyze.

Sometimes, the same CME is observed at different locations by two (or, rarely, three) spacecraft. We refer to this instance as a measurement with spacecraft in conjunction. In the case of an almost radial alignment, the evolution of the CME properties can be investigated (Leitner et al. 2007; Nakwacki et al. 2011; Good et al. 2019; Salman et al. 2020b; Davies et al. 2022). Such conjunctions are relatively rare in the inner heliosphere (~0.3–1.5 au). Most studies are limited by the required assumption that the same part of the CME is being observed. In addition, the evolution of the CME due to its interactions with the solar wind and corotating structures (Winslow et al. 2016; Davies et al. 2020) cannot be easily distinguished from the internal evolution of the CME (Lugaz et al. 2020; Davies et al. 2021b).

An additional difficulty is that the CME continues to evolve as it passes over a spacecraft. Near 1 au, an ME duration is typically around 20 hr (Nieves-Chinchilla et al. 2018), which is about 25% of its age. The effect of the temporal evolution of the CME properties over the duration of the spacecraft crossing is referred to as the aging effect (Osherovich et al. 1993). It causes difficulties in computing and deriving some of the properties of the ME in situ profile, such as its average magnetic field strength and the asymmetry of its profile, among others. As noted previously by Klein & Burlaga (1982), the speed profile of MEs as measured in situ is often decreasing as it passes over the spacecraft, which is typically interpreted as a result of ME expansion and can be corrected using assumptions regarding the expansion (Farrugia et al. 1993). Démoulin et al. (2020) developed a methodology to deduce the instantaneous magnetic field strength profile of MEs by quantifying the expansion using a fit of the speed within the ME assuming a self-similar expansion. Their methodology assumes that all of the change in the velocity as the ME passes over the spacecraft is due to expansion and corrects for it. This method neglects the changes due to the global evolution of the ME; e.g., the ME center speed may decrease during the time taken for the ME to pass over the spacecraft. Hereafter, we distinguish between changes due to expansion and those due to aging, as described in Osherovich et al. (1993).

Rarely, the same CME is probed simultaneously by more than one spacecraft (Farrugia et al. 2011; Kilpua et al. 2011; Winslow et al. 2021; Lugaz et al. 2022). When this is the case, the CME is typically measured by two spacecraft at approximately the same distance but separated by an azimuthal angle ranging from a fraction of a degree to 40°-50°. With such spacecraft configurations, it is possible to gain direct information about the global structure of MEs, for example,

whether the assumption of axial invariance is valid (Möstl et al. 2009a, 2009b; Mulligan et al. 2013), but such conjunctions have been limited to a few cases (Lugaz et al. 2018).

There has not been, to the best of our knowledge, any study looking at simultaneous measurements of CMEs by two (or more) spacecraft at different radial distances but approximately aligned in longitude. This configuration is the same as for the investigations of CME evolution discussed above but for spacecraft in relatively close radial proximity. Since an ME is typically about 0.2 au in radial extent at 1 au (Lepping et al. 1990), we select events where spacecraft are radially separated by less than 0.2 au. Such measurements enable, in the case of a radial alignment, the investigation of the CME's temporal evolution (aging) rather than its radial evolution (propagation). The types of simultaneous measurements on which we focus here can significantly improve our understanding of the complex magnetic structure of MEs and help us, for instance, to quantify the aging and expansion processes occurring during the ME crossing. We further discuss the insights gained by the different spacecraft configurations in Section 5.

The aim of this paper is to take advantage of such simultaneous measurements. We do so, first, by investigating how consistent the ME properties are when measured simultaneously by two spacecraft with small radial separation and, second, by quantifying the aging effect and proposing ways to reduce it. The latter allows us to deduce instantaneous CME properties and thus have a better understanding of the ME structure.

To find such events measured simultaneously by two spacecraft with small but nonnegligible radial separations and small angular separations (that include latitudinal and longitudinal separations), we search more than 4 decades of data for instances where two spacecraft measured the same CME at the same time. In Section 2, we describe our procedure to identify such events. These events are referred to as "simultaneous measurements." In Section 3, we first show an example of a simultaneous measurement event and then analyze all of the events at our disposal in terms of typical differences between the two spacecraft. We focus on the magnetic field strength and the asymmetry of its temporal profile. This enables us to conclude that the differences are not primarily due to radial propagation but must be a combination of temporal changes (aging) and geometrical effects. In Section 4, we present a case study of a simultaneous measurement, allowing us to quantify for the first time the effect of aging on in situ profiles. We also use this case to investigate two methods to reduce this effect. In Section 5, we show what can be done given different spacecraft configurations during simultaneous measurements. Finally, in Section 6, we conclude and discuss our findings.

2. Simultaneous Measurement Catalog

We use existing catalogs of CMEs measured in the inner heliosphere to identify events measured by two spacecraft with moderate separations and an automated algorithm (see below for quantitative explanations) to search the catalog for such events. Combined, these catalogs represent a total of 2374 potential CMEs spread over more than 4 decades of data acquisition by 11 different interplanetary probes. Some CMEs may appear in multiple lists, for example, in the list of CMEs measured by ACE of Richardson & Cane (2010) and the HELIO4CAST ICMECAT list of Möstl et al. (2020) covering CMEs measured by Wind. However, if a duplicate of the same CME is found after all of the filtering processes described in the

next section, we manually remove it from the list of potential simultaneous measurements.

The list of CME catalogs used in this study is as follows.

- 1. Combined HELIO4CAST ICMECAT^{3,4} catalog of CMEs of Möstl et al. (2017, 2020), where we focused on events measured by BepiColombo, Parker Solar Probe, Solar Orbiter, MESSENGER, ACE/Wind, STEREO-A, and STEREO-B; 1073 CMEs from 0.05 to 1 au; 1995–2021.
- 2. Richardson & Cane (2010), ACE; 531 CMEs at 1 au; 1996–2022.
- 3. Wang et al. (2005), Helios-1, Helios-2, Pioneer Venus Orbiter (PVO), ACE; 596 CMEs from 0.3 to 1 au; 1975–2003.
- 4. Cane et al. (1997), Helios-1, Helios-2; 29 CMEs from 0.3 to 1 au; 1975–1978.
- 5. Davies et al. (2022), Wind, Juno; 27 conjunctions from 1 to 2 au; 2011–2014.
- Mulligan et al. (1999), Near Earth Asteroid Rendezvous (NEAR), Wind; four conjunctions from 1 to 1.6 au; 1997.
- 7. Jian et al. (2008), PVO; 124 CMEs from 0.72 to 0.73 au; 1979–1988.

To identify CMEs measured by two spacecraft with close spatial separations, we use the position (using the interpolated daily position obtained at https://omniweb.gsfc.nasa.gov/coho/helios/heli.html) of the spacecraft at the time of a detected CME and look for the position of the other spacecraft. We take the trajectory of the Earth for all spacecraft at L1 and the Venus trajectory for the PVO mission once it entered orbit around Venus in 1978 December (Colin 1980).

If, during a CME encounter with a spacecraft, another spacecraft has a radial separation of less than 0.2 au and an angular separation ($\Delta \alpha$) lower than 10°, we flag this event as a potential simultaneous measurement. The angular separation is the angle between the two Sun-spacecraft lines in 3D space. It is dominated by the longitudinal separation between the spacecraft, since most spacecraft orbit in the ecliptic plane, but also includes the latitudinal separation. We compute it using the dot product of the two spacecraft position vectors. We do not set a lower limit for the radial separation because it is difficult to determine a threshold value related to the CME radial size at different distances from the Sun, and we do not want to exclude possible interesting cases. We instead manually remove the events for which the two spacecraft are too close (see details below). For CMEs detected at L1 after 1995, we use ACE or Wind data when they are available and depending on which spacecraft the CME has been reported on in the database (all CMEs should be observed by both, except when Wind was inside Earth's magnetosphere during the first few years of the mission). For CMEs before 1995, we use the IMP-8 spacecraft. We do not consider cases where the CME was only measured by spacecraft at or near L1, for example, simultaneous measurements by ACE, Wind, and IMP-8, since the separation between the spacecraft is too small to have any effect on the interpretation of the large-scale structure of MEs. For example, Lugaz et al. (2018) showed that the measurements are nearly identical up to separations of $\sim 200 R_{\rm E}$ (i.e., $\sim 0^{\circ}4$).

We find 126 potential simultaneous measurements satisfying these criteria for the radial and angular separations. This initial list does not take into consideration whether data are available at both spacecraft. They are found using only the positions of the spacecraft. A significant portion of these potential simultaneous measurements occurs during the early cruise phase of planetary missions, when data may not be available.

In a second step, we visually inspect these 126 events and remove all those for which there are no available data at one of the spacecraft or cases where the two spacecraft are too close (for example, the 2006 December 13 CME measured by the two STEREO spacecraft and ACE and Wind just after the launch of the STEREO spacecraft). We then confirm that there is a temporal overlap between the measurements because, for example, a small CME may not be measured simultaneously by two spacecraft separated by 0.2 au. We also removed potential events where the CME signatures (mainly low proton β and a smooth magnetic field) are clear at only one of the spacecraft.

Table 1 presents the catalog of the final 19 CME events for which there are multispacecraft simultaneous measurements. We generally use the ME boundaries as provided in existing catalogs except for some MEs for which we adjusted the boundaries following visual inspection so that MEs at both spacecraft have consistent boundaries. Thus, for the measurements at the second spacecraft, we attempt to match the features observed at the first spacecraft profile with those of the second one. Note that, in almost all cases, we only have plasma data at one of the spacecraft, making it important to define boundaries primarily through discontinuities in the magnetic field vector. We would like to note that the MEs presented in this catalog are complicated, and with the lack of plasma measurements in most of the MEs, the boundaries can be difficult to identify clearly.

All of the MEs in Table 1 are probed at approximately the same time by the two spacecraft. The results presented in Section 3 are focused on the overall properties (such as the ME mean magnetic field) that are the least affected by the accuracy of the defined boundaries. The table also lists the overlapping duration, i.e., the duration during which both spacecraft are simultaneously inside the ME, as a percentage of the ME duration at SC1, which ranges from 18% to 100% (median of 73%). The table also gives the distance from the Sun of both spacecraft (in au) and the angular separation (in degrees), which includes both the longitudinal and latitudinal separations. Depending on the value of the overlap, different studies can be performed as detailed in Section 5.

In Table 2, from left to right, we list the event ID, mean magnetic field (in nT), maximum magnetic field (in nT), distortion parameter (DiP; see Nieves-Chinchilla et al. 2018), and front-to-back ratio observed at both spacecraft. The DiP quantifies the asymmetry of the magnetic field profile by giving the location within the ME where half the total magnetic flux is reached. A value of DiP = 0.5 indicates a symmetric ME for this particular measure of asymmetry. A DiP lower than 0.5 corresponds to an ME with a magnetic field stronger in the first half of its profile, and vice versa. Such a feature is often interpreted as the result of a compression of the ME structure (see, e.g., Masías-Meza et al. 2016; Janvier et al. 2019). We define the front-to-back ratio as the ratio of the ME magnetic field strength averaged over the front 10% (by duration) divided by the back 10% (by duration) of the ME magnetic field profile.

https://helioforecast.space/icmecat

⁴ https://doi.org/10.6084/m9.figshare.6356420.v12

 Table 1

 Catalog of the 19 Events with Simultaneous Spacecraft Measurements

No.	SC1	SC2	ME Start1	ME End1	ME Start2	ME End2	Overlap (%)	r1 (au)	r2 (au)	$\Delta \alpha$ (deg)
1	Solar Orbiter	Wind	2021-11-04T07:09	2021-11-04T19:38	2021-11-04T10:52	2021-11-05T04:14	70.3	0.84	0.99	2.2
2	Helios-2	IMP	1978-01-04T07:07	1978-01-05T14:51	1978-01-04T10:54	1978-01-05T16:00	88.1	0.94	0.98	5.6
3	IMP	Helios-2	1978-01-06T01:06	1978-01-06T16:53	1978-01-06T01:16	1978-01-06T14:47	99.0	0.98	0.95	6.2
4	Helios-1	IMP	1975-11-17T04:45	1975-11-17T18:08	1975-11-17T12:02	1975-11-17T23:35	45.5	0.86	0.99	5.1
5	Wind	NEAR	1997-12-10T18:35	1997-12-12T00:04	1997-12-11T18:46	1997-12-12T23:33	18.0	1.00	1.18	1.2
6	Wind	Juno	2011-09-17T15:35	2011-09-18T08:51	2011-09-17T20:00	2011-09-18T14:43	74.4	1.00	1.07	6.6
7	Wind	Juno	2011-09-26T20:54	2011-09-28T14:14	2011-09-27T09:54	2011-09-28T23:30	68.5	0.99	1.11	7.7
8	Wind	Juno	2011-10-05T09:56	2011-10-07T02:06	2011-10-05T21:32	2011-10-07T10:22	71.1	0.99	1.14	6.8
9	Wind	Juno	2013-10-30T17:34	2013-10-31T05:00	2013-10-31T02:32	2013-10-31T23:47	21.6	0.98	1.10	4.9
10	Wind	Juno	2013-11-11T17:44	2013-11-12T01:56	2013-11-11T22:58	2013-11-12T08:06	36.1	0.98	1.18	4.5
11	STEREO-A	PSP	2019-11-02T21:19	2019-11-03T22:02	2019-11-02T21:58	2019-11-03T18:12	97.4	0.96	0.92	2.7
12	ACE	STEREO-B	2007-06-08T05:45	2007-06-09T05:15	2007-06-08T05:45	2007-06-09T08:14	100.0	1.01	1.07	4.2
13	STEREO-B	STEREO-A	2007-05-22T04:26	2007-05-23T03:52	2007-05-22T14:00	2007-05-23T13:30	59.2	1.06	0.96	9.1
14	ACE	STEREO-A	2007-05-22T05:08	2007-05-23T13:30	2007-05-22T14:00	2007-05-23T13:30	72.6	1.01	0.96	6.0
15	STEREO-A	ACE	2007-03-29T13:29	2007-03-29T20:37	2007-03-29T15:04	2007-03-30T00:03	77.9	0.97	1.00	2.1
16	ACE	STEREO-B	2007-03-29T15:04	2007-03-30T00:03	2007-03-29T18:24	2007-03-30T03:54	62.8	1.00	1.02	0.7
17	ACE	STEREO-A	2007-01-15T21:55	2007-01-16T03:50	2007-01-15T22:16	2007-01-16T03:01	94.3	0.98	0.97	0.7
18	STEREO-A	STEREO-B	2007-01-14T11:57	2007-01-15T08:21	2007-01-14T12:23	2007-01-15T07:55	97.8	0.97	0.98	0.1
19	ACE	STEREO-B	2007-01-14T11:46	2007-01-15T07:37	2007-01-14T12:10	2007-01-15T07:37	98.0	0.98	0.98	0.3

Note. From left to right: times of entry into the ME of the first and last spacecraft, distances from the Sun for both spacecraft (in au), start and end times for both spacecraft (in YYYY-MM-DDThh:mm format), overlapping time expressed as a percentage of the ME duration at SC1, and angular separation (in degrees).

3. Comparison of the ME Properties between the Two Spacecraft

Taking advantage of the proximity of two spacecraft observing the same CME, we now show how different the ME properties can be for angular separations of less than 10° and radial separations of less than 0.2 au. We first describe an example of a simultaneous measurement event and then generalize the method used on this event to the 19 events present in our catalog.

3.1. Wind–Juno ME of 2011 September 17

Figure 1 presents the magnetic and plasma data for one of the CMEs studied in Davies et al. (2021a, 2022). Green corresponds to Wind measurements and orange to Juno. The ME reached Wind on 2011 September 17. The two spacecraft had a radial separation of 0.07 au, with Juno around 1.07 au, and an angular separation of 6°6. At this angular separation, we expect some significant differences, especially in the magnetic field components based on previous studies (Kilpua et al. 2011; Lugaz et al. 2018). This is a relatively slow ME with a speed of \sim 440 km s⁻¹ and no radial expansion, as seen from the velocity measurements observed by Wind presented in the last panel. The ME is preceded by a shock (impacting Wind at 02:57 UT) and a dense sheath region (not shown here). We observe clear shock signatures in the in situ measurements both at Wind and at Juno. The beginning of the ME is highlighted by the sudden decrease of B_T and B_N and the increase of B_R at both spacecraft. The end of the ME is chosen to correspond to the time when the magnitude of the magnetic field increases suddenly at both spacecraft after an almost monotonic decrease.

The total magnetic field strength profile of the ME has a bell-like shape similar to what would be expected in typical force-free MC models (Lundquist 1951; Marubashi 1986; Vandas & Romashets 2003). However, the position of the maximum of

the magnetic field within the ME is different at Wind and Juno; the maximum is closer to the ME leading edge at Wind than it is at Juno. This is also reflected by the DiP, which shows a very asymmetric profile at Wind (DiP of 0.40) and a nearly symmetric profile at Juno (DiP of 0.48). Because the decrease of the magnetic field strength in the back of the ME is larger at Wind than at Juno, the average magnetic field increases with heliocentric distance, from 10.3 nT at Wind to 11.5 nT at Juno. However, the peak magnetic field strength is quite similar at both spacecraft.

Different physical mechanisms could be responsible for the shift of the peak toward the center of the ME from Wind to Juno. As already discussed in previous studies (e.g., see Farrugia et al. 1993; Janvier et al. 2019), the magnetic field profile of MEs tends to become more symmetric as the MEs propagate away from the Sun due to relaxation toward a forcefree state. However, here this effect would need to take place over just a few hours (4.4 hr between the beginning of the ME at the two spacecraft), so relaxation cannot explain the changes within such short timescales. Indeed, in a magnetized plasma, the maximum speed at which information can propagate is at the fast magnetosonic speed, $\sqrt{v_a^2+c_s^2}$, where v_a and c_s are the Alfvén speed and the speed of sound, respectively. For an ME relaxation to occur, we expect that the waves in the ME have enough time to propagate in the entire ME size at least once. The ME size is 0.25 au using the average speed of the ME at Wind, while the average fast magnetosonic speed is 153 km s⁻¹ in the ME at Wind. Within the 4.4 hr delay between the ME front at Wind and Juno, the waves only have time to travel about 0.02 au. This corresponds to a very small portion of the ME. Thus, we conclude that relaxation of a large-scale transient such as a CME does not have time to occur from Wind to Juno, since information does not have time to propagate far enough.

From the Wind plasma measurements, there is no indication that a fast or dense solar wind stream is following this ME. We

Table 2
ME Properties Measured by the Two Spacecraft

No.	ID	Bmean1 (nT)	Bmean2 (nT)	Bmax1 (nT)	Bmax2 (nT)	DiP1	DiP2	Ratio1	Ratio2
1	SolarOrbiter_Wind_2021-11-04	18.2	14.5	19.2	16.1	0.50	0.49	1.0	1.0
2	Helios-2_IMP_1978-01-04	17.2	14.4	21.0	16.4	0.47	0.54	1.5	1.0
3	IMP_Helios-2_1978-01-06	12.1	13.2	14.9	15.3	0.48	0.47	1.3	1.6
4	Helios-1_IMP_1975-11-17	12.8	14.3	14.5	15.4	0.58	0.49	0.7	1.1
5	Wind_NEAR_1997-12-10	11.7	8.8	16.3	13.1	0.40	0.42	2.1	2.1
6	Wind_Juno_2011-09-17	10.3	11.5	14.1	15.0	0.40	0.48	2.8	1.4
7	Wind_Juno_2011-09-26	6.3	7.7	13.9	14.7	0.41	0.37	2.4	1.9
8	Wind_Juno_2011-10-05	10.5	8.3	14.8	11.1	0.44	0.47	1.8	1.6
9	Wind_Juno_2013-10-30	8.9	7.6	10.9	9.3	0.48	0.47	1.0	1.3
10	Wind_Juno_2013-11-11	7.2	7.8	7.5	8.6	0.51	0.49	0.9	1.2
11	STEREO-A_PSP_2019-11-02	6.4	6.6	7.4	8.4	0.52	0.56	0.8	0.7
12	ACE_STEREO-B_2007-06-08	7.6	7.3	9.7	11.7	0.50	0.54	0.9	0.7
13	STEREO-B_STEREO-A_2007-05-22	12.5	9.6	17.6	11.8	0.44	0.56	1.0	0.8
14	ACE_STEREO-A_2007-05-22	9.2	9.6	16.4	11.8	0.45	0.56	1.3	0.8
15	STEREO-A_ACE_2007-03-29	4.6	4.7	5.9	6.3	0.59	0.57	0.5	0.6
16	ACE_STEREO-B_2007-03-29	4.7	4.3	6.3	5.8	0.57	0.58	0.6	0.5
17	ACE_STEREO-A_2007-01-15	7.7	7.4	9.6	8.9	0.45	0.46	1.2	1.4
18	STEREO-A_STEREO-B_2007-01-14	11.5	11.5	14.9	14.7	0.56	0.57	0.5	0.4
19	ACE_STEREO-B_2007-01-14	11.4	11.4	14.8	14.7	0.56	0.57	0.5	0.4

Note. From left to right, the columns show the event ID (date at which the first spacecraft observed the ME), where the spacecraft are listed in the order in which they entered the ME; mean magnetic field inside the ME (in nT); maximum magnetic field strength measured within the ME; DiP; and front-to-back ratio. Labels 1 and 2 correspond to the first and second spacecraft to enter the ME, respectively.

note that the two spacecraft are 6.6 (0.12 au of arc length) apart, so this difference in the asymmetry of the magnetic field could be due to inhomogeneous and thus denser solar wind material at Wind than at Juno that locally compresses the magnetic structure. To verify this statement, one would need the plasma data at Juno, which are not available at that time. We also want to point out that, following the linear force-free paradigm (thus with an invariant axis), we cannot explain the shift of the peak of the magnetic field strength profile (even considering different ME inclinations) from Wind to Juno and the differences we observe in the magnetic field components with an angular separation of 6.6 between the spacecraft.

The particular ME presented in this section shows that an angular separation of 6.6 between spacecraft is enough to result in significant differences in the mean magnetic field strength and the asymmetry of its profile. We now extend this comparison to the 19 CMEs presented in our catalog.

3.2. Magnetic Field Strength

For the ME events in our catalog, the two spacecraft are separated by up to 10° and 0.2 au; thus, the spacecraft may sample different parts of the ME at the same time and observe significant differences in the mean magnetic field strength. Figure 2 shows scatter plots of the mean magnetic field strength of the ME as a function of the radial distance and absolute angular separation (α) , respectively. The two observation points of the same ME are connected with a line. Each event is plotted using a different color.

As MEs propagate in the heliosphere, their magnetic field strength decreases (Bothmer & Schwenn 1998; Liu et al. 2005; Wang et al. 2005; Richardson 2014; Winslow et al. 2015; Lugaz et al. 2020; Davies et al. 2021a). This decrease is typically fitted by a power law with a radial distance with an index between -1 and -2. However, if we study the changes of the ME magnetic field strength on shorter length scales (and

shorter timescales), this is not what we observe all the time. The black and gray dashed lines in panel (a) show past power law relationships of the magnetic field strength as a function of the radial distance deduced in Winslow et al. (2015) and Davies et al. (2021a), respectively, where B is the magnetic field strength, and r is the heliocentric distance. We take the following two evolution laws of the mean magnetic field as a function of the heliocentric distance: $B = 7.46r^{-1.95}$ from Winslow et al. (2015) and $B = 9.19r^{-1.62}$ from Davies et al. (2021a). Changes of the ME properties that differ from these power laws have also been discussed for single events observed by multiple spacecraft at different distances from the Sun (Good et al. 2019; Salman et al. 2020b; Davies et al. 2022). Here, for six cases, the average magnetic field is actually found to be larger at the spacecraft taking the measurements at a further radial distance. This highlights that, for radial separations of 0.04–0.2 au between two spacecraft, the changes in the measured ME properties can be significant and may not be primarily due to the ME propagation. This can be explained as due to either (i) the effects of the different crossing distances from the ME axis within the paradigm of MEs as cylindrical flux ropes with a straight axis; (ii) the effects of different crossings through a more complex and distorted ME, for example, without a straight axis; or (iii) physical processes happening within shorter timescales than the Sun-to-Earth propagation time, for example, interaction with a following fast solar wind stream. We refer to the first two processes as being due to the 3D nature of the ME structure. Note that the variation of the mean magnetic field strength over these small radial separations has large event-to-event variability without a clear overall trend; therefore, no final conclusion about any trend can be reached.

Using Table 2, we find that the mean and median of the absolute difference of the average ME magnetic field are 1.3 and 1.0 nT, respectively. This result gives an estimate of the typical difference in the average magnetic field measured by

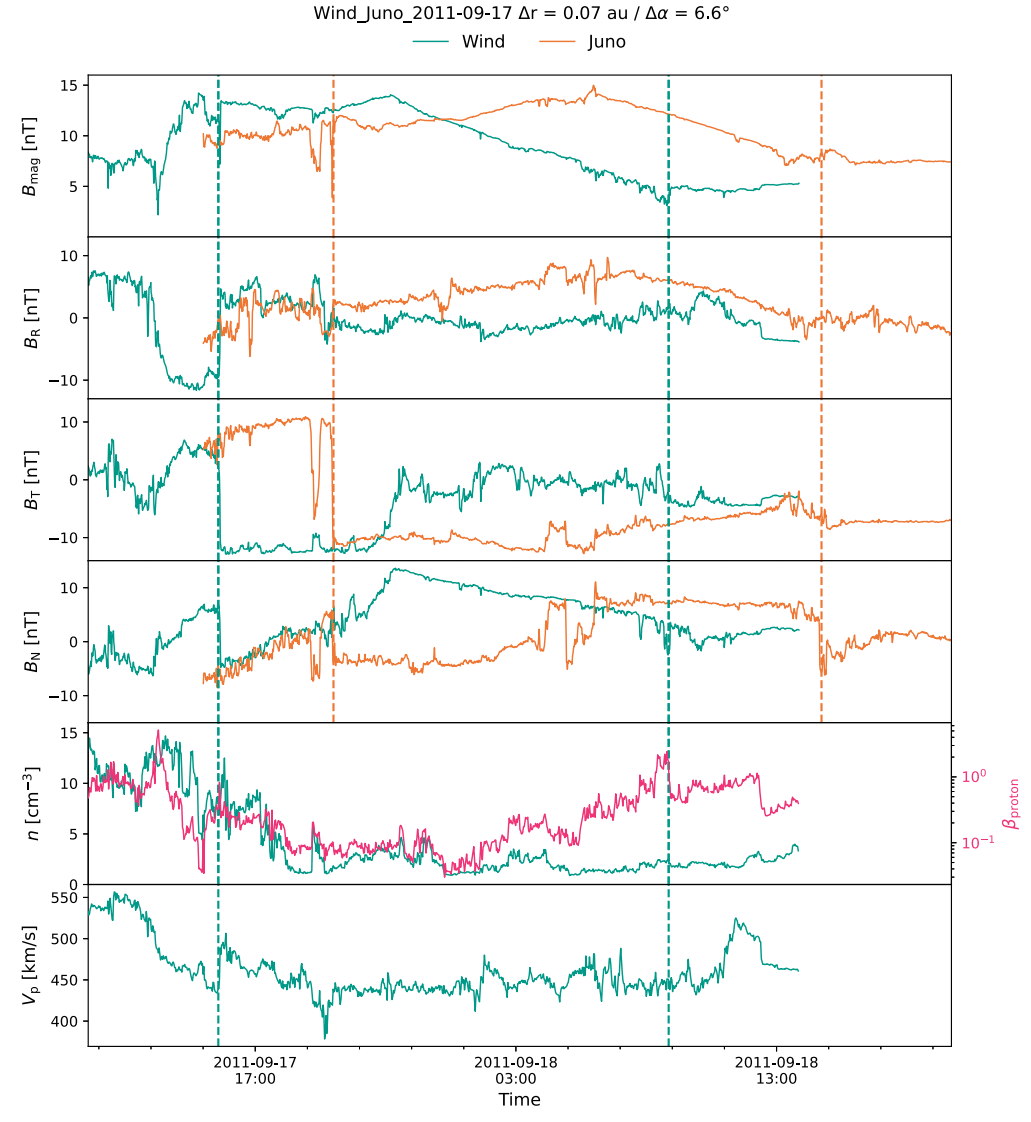


Figure 1. In situ measurements of the 2011 September 17 CME observed at Wind (green) and Juno (orange). The panels show, from top to bottom, the magnitude of the magnetic field and its components in RTN coordinates in nT, the density in cm⁻³, the proton β parameter (red), and the speed in kilometers per second.

two spacecraft separated by small angular and radial separations near 1 au $(\pm 10^{\circ}$ and 0.2 au).

We note that we only looked at events with angular separations of less than 10° and that there is no clear association between the increase in magnetic field and the angular separation of the two spacecraft. It is possible that our results are inconclusive due to low statistics. It also raises the question of the geometry of MEs and their magnetic coherence, in particular, because we also find significant scatter of the mean ME magnetic field as a function of the angular separation. We focus here solely on the average magnetic field strength, not the magnetic field components. Previous work (e.g., see Lugaz et al. 2018) has shown that the correlation of the total magnetic field strength between two spacecraft decreases much more slowly with angular separation than the correlation of the components.

3.3. ME Distortion

Figure 3 summarizes the differences between the ME properties measured by each of the two spacecraft for the 19 events under study. Panel (a) shows the DiP parameter, and

panel (b) shows the front-to-back ratio of the magnetic field strength measured at each spacecraft for each ME measured simultaneously by two spacecraft. In the background, the blue histograms show the absolute difference of the DiP (or the front-to-back ratio) between the two spacecraft. We use the blue histogram in panel (a) of Figure 3 to compute the average of the absolute difference of the DiP. This allows us to estimate the typical differences of the asymmetry of the magnetic field for small angular and radial separations near 1 au. The mean value of these differences is 0.04, and the median value is 0.02.

A value of 0.4 for the DiP corresponds to an almost linear magnetic field decrease, with the magnetic field at the front 2.1 times stronger than that at the rear, as shown by Figure 4 (the Wind_NEAR_1997-12-10 case, discussed later in this paper). Such a DiP value corresponds to a strongly asymmetric magnetic profile. The mean difference in DiP of 0.04 between the two spacecraft found for the events in our study, therefore, corresponds to a measurable change in the magnetic field profile asymmetry between two spacecraft taking simultaneous measurements, amounting to about 8%–10% of typical values. This highlights that the differences in the ME properties

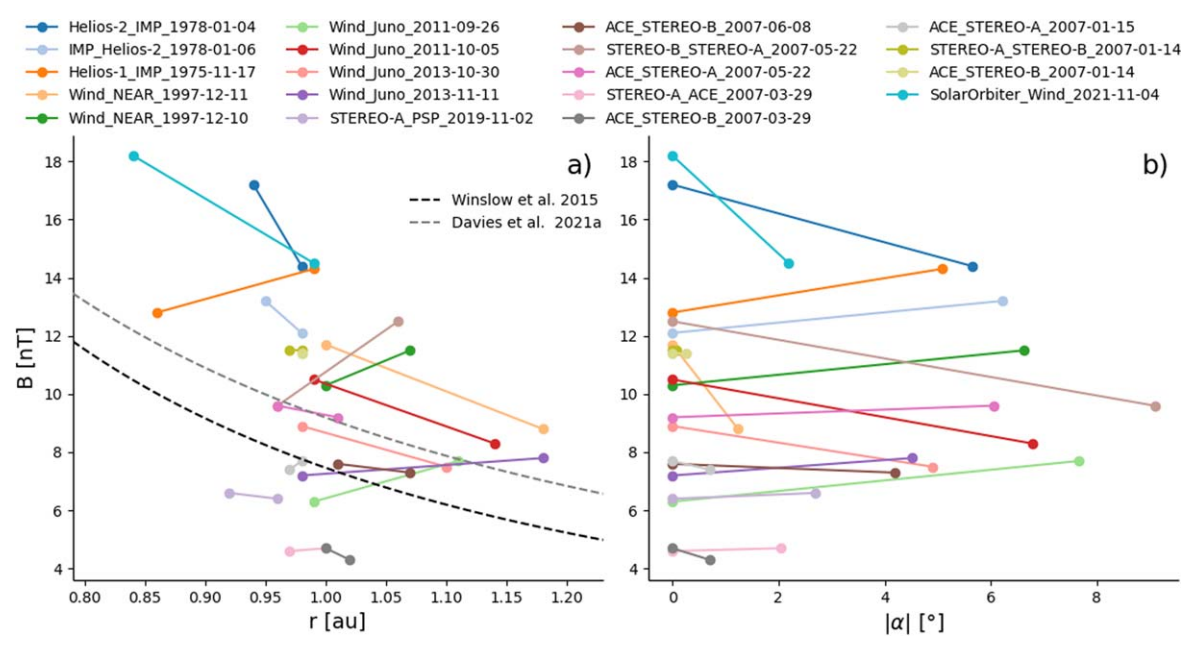


Figure 2. Mean magnetic field (in nT) of the ME as a function of the radial distance (in au; panel (a)) and angular separation (in degrees; panel (b)).

between the two spacecraft are significant, even for these small separations.

We find that, for five events, the ME was first measured by the spacecraft that is further from the Sun. This suggests either local distortion of the ME by interaction with the solar wind, significant tilt of the ME front, or nonradial propagation due to a potential CME deflection. In some cases, it could also be explained if the two spacecraft cross the ME with different impact parameters, but this interpretation would require the five MEs in this case to be inclined, since the two spacecraft are separated primarily in longitude, not latitude.

We compute the Pearson and Spearman correlation coefficients for the DiP and the front-to-back ratio, and we find values of -0.87 and -0.90, respectively. Therefore, there is a very good anticorrelation between the front-to-back ratio and the DiP parameter in the catalog of simultaneously measured MEs. The front-to-back ratio is thus a good proxy for the overall asymmetry of the magnetic field strength profile. We return to this when investigating the ME instantaneous profile.

4. Quantifying the Aging Effect and Ways to Reduce it

In the rest of this study, we take advantage of simultaneous measurements to quantify one of the physical processes that may have a significant effect during the crossing of a CME over a spacecraft: aging. We define it as the effect of the CME temporal evolution on the in situ parameter profile during its propagation. Aging can manifest itself in terms of local processes, such as magnetic reconnection, or more global ones, such as a deformation of the cross section occurring during the time when the spacecraft probes the CME. Such phenomena can impact observed CME properties, such as the asymmetry of the magnetic field strength profile. While we do not focus on the ME velocity due to the paucity of measurements, CME deceleration as it passes over a spacecraft is another example of aging that may affect the quantification of CME expansion.

We look in detail at one ME observed by Wind and NEAR. During the passage of this particular CME, the configuration of the two spacecraft allows us, for the first time, to quantify the aging effect using the asymmetry of the magnetic field profile in Section 4.2. We then present two methods that aim to reduce this aging effect and compare the results in Sections 4.3 and 4.4.

4.1. An ME Observed by Wind and NEAR on 1997 December 10

Figure 4 presents the measurements for one of the CMEs studied in Mulligan et al. (1999) using NEAR and Wind measurements while these two spacecraft are almost radially aligned ($\Delta \alpha = 1^{\circ}2$). The ME reached Wind on 1997 December 10. The radial separation of the two spacecraft was 0.18 au (i.e., NEAR was at 1.18 au), similar to the typical size of an ME near 1 au. While both spacecraft measured the magnetic field, plasma measurements are only available at Wind. The ME at Wind is associated with a lower density and proton β than the nearby solar wind (penultimate panel), clearly highlighting a magnetically dominated structure. The velocity profile at Wind (last panel) is complex and does not show the clear decreasing profile that is common for most MEs near 1 au. The ME front speed is, however, slightly higher than the back by about 30 km s⁻¹, indicating a small radial expansion. The ME is preceded by a shock and a relatively long sheath lasting about 14.5 hr (not shown here). Part of the magnetic data was not available when the ME was passing over NEAR. However, there are a few data points at NEAR right before the increase in the total magnetic field strength (due to the increase of B_N). This feature is also visible at Wind and shows the end of the ME. We thus decide to put the ME end for NEAR at this time. Moreover, we perform a linear interpolation of the missing data at the back of the NEAR ME for the magnetic field strength as it decreases in an almost linear fashion toward the back of the Wind ME.

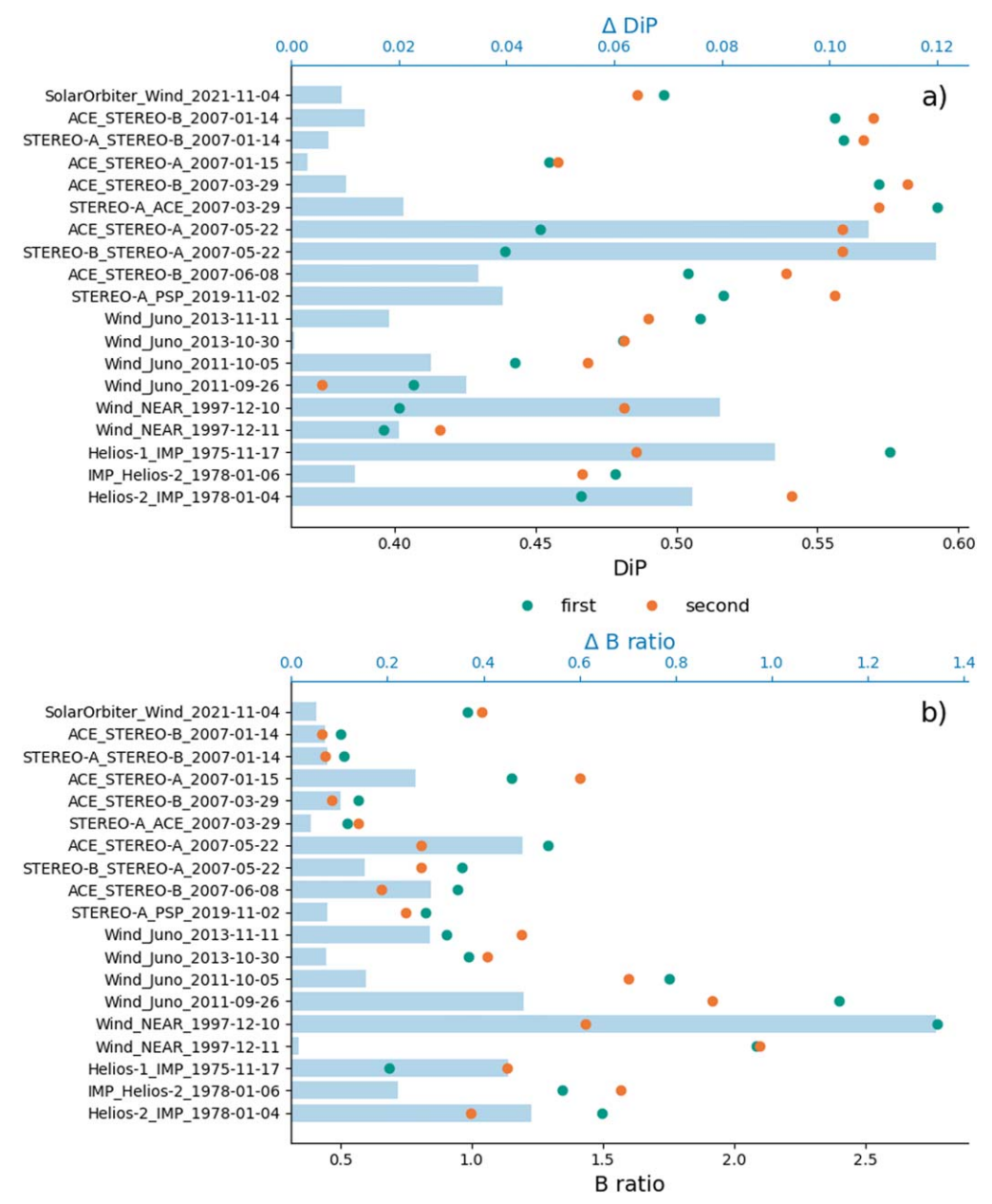


Figure 3. Summary plot of the catalog of MEs measured simultaneously by two spacecraft. Panels (a) and (b) show the DiP and front-to-back ratio measured at both spacecraft, respectively, for all events (green and orange data points; bottom scale) and the absolute value of the difference between the two spacecraft (blue histograms; top scale).

More details about the event can be found in Mulligan et al. (1999). Here our focus is on the simultaneous measurements and what they reveal about the ME temporal evolution during the passage over the spacecraft. To do so, we turn our attention to the magnetic field measurements inside the ME. Both spacecraft measure an ME with similar magnetic field components, specifically for B_T and B_N . More analysis of the orientation of the ME can be found in Mulligan et al. (1999). We now focus on the magnetic field strength, whose value does not depend on the transformation of the magnetic field components into the same coordinate system and which has been found to be coherent over wider longitudinal separations than the magnetic field components. The temporal profile of the magnetic field strength at Wind shows a strong asymmetry, with an almost linear decrease within the ME. A similar behavior is visible at NEAR. The DiP at Wind is

0.40, whereas it is 0.42 at NEAR. Such an asymmetry is typically associated with strongly expanding MEs; however, this is not the case for this event, as the ME speed at Wind shows little indication of any radial expansion. This clearly indicates that radial expansion cannot be the main cause for this asymmetry. The average magnitude of the magnetic field inside the ME is 25% lower at NEAR as compared with Wind (8.8 nT compared to 11.7 nT). This decrease occurs over a radial distance of 0.18 au, corresponding to a propagation time of 24 hr. This is comparable to the duration of the ME at Wind (29.5 hr). It gives a strong indication that the assumption of the CME as a static structure as it passes over the spacecraft is not justified, even in the absence of significant radial expansion, as is the case here. This result suggests that, while propagating from Wind to NEAR, the CME has not expanded significantly, but it has aged. This is also consistent with the

Wind_NEAR_1997-12-10 $\Delta r = 0.18$ au / $\Delta \alpha = 1.2^{\circ}$

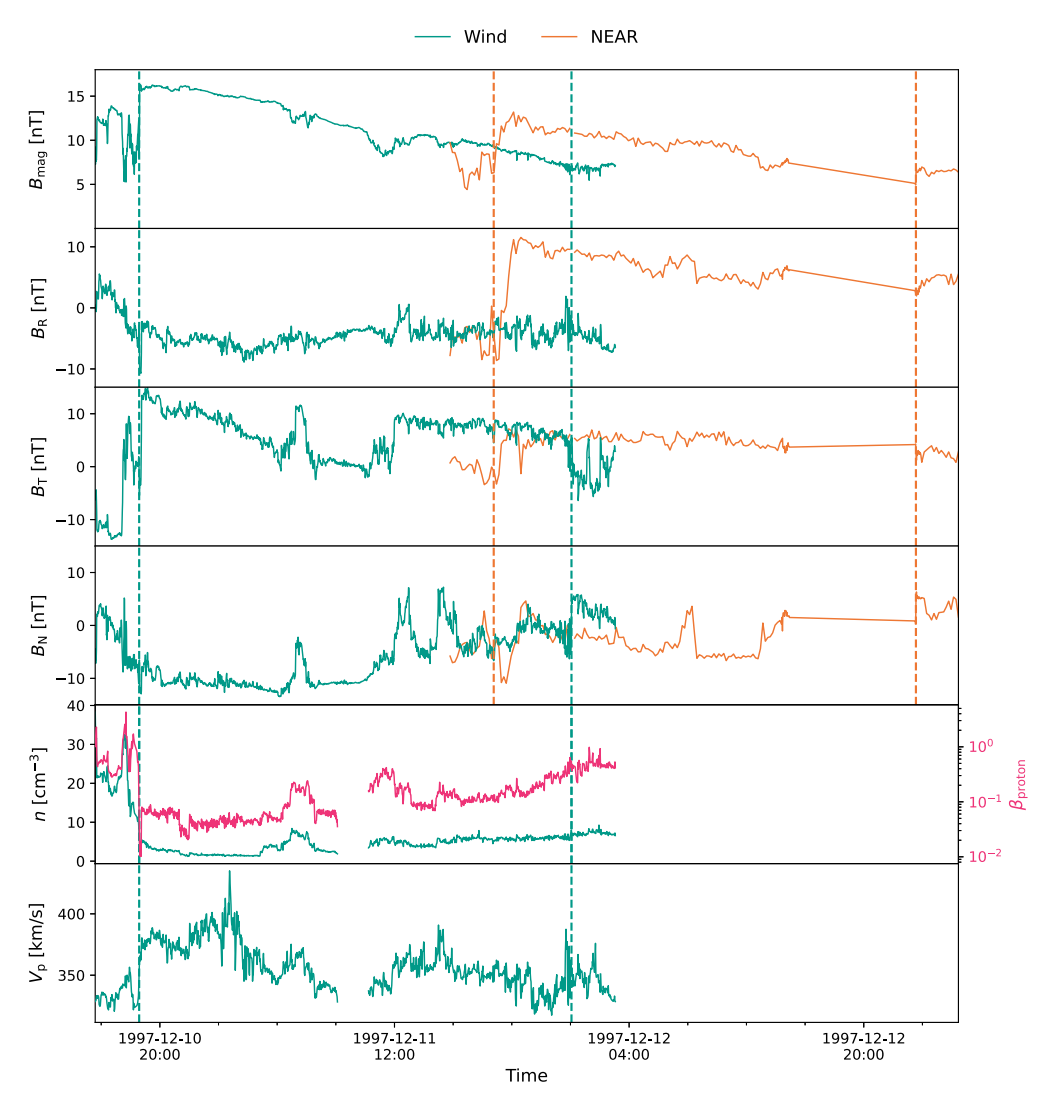


Figure 4. In situ measurements of the 1997 December 10 CME observed at Wind (green) and NEAR (orange), presented in the same format as Figure 1.

nearly equal durations at both spacecraft. We return to this point in Section 4.2.

4.2. ME Instantaneous Asymmetry

In the analysis presented so far, we have not taken full advantage of the fact that the two spacecraft are measuring the ME at the same time but in different locations. Here we turn our attention to these simultaneous measurements and how they can help us better understand the true morphology of the MEs.

In the Wind-NEAR event presented in Figure 4, the spacecraft are in a configuration such that NEAR measures the front of the ME at the exact same time that Wind is measuring the back of the ME, while the angular separation between the spacecraft is very small. We note that, as only measurements at the front of the ME at NEAR are used, the definition of the ME end at NEAR does not impact our results. We thus have simultaneous measurements of the magnetic field at the front (probed by NEAR) and the back (probed by Wind) of the ME. With such a configuration, we can then compute an instantaneous front-to-back ratio by combining the CME measurements taken by the two spacecraft, thus removing

any effect of the ME temporal evolution. As discussed in Section 3, the front-to-back ratio is a good proxy for the overall asymmetry of the profile.

Computing the instantaneous front-to-back ratio during the overlapping time gives us 1.4. The front-to-back ratio of the original profiles is 2.1 at both Wind and NEAR. We see here that single-spacecraft measurements lead us to strongly overestimate the asymmetry of the magnetic field profile.

4.3. Correcting for Expansion

Panel (a) of Figure 5 depicts the "instantaneous" expansion-corrected profile of the ME obtained using the Démoulin et al. (2020) methodology for the Wind-NEAR event. This method quantifies the effect of radial expansion on the ME magnetic field. To do so, we perform a linear fit to the speed inside the ME and use the result to compute the parameter f that quantifies the expansion, assuming a self-similar expansion and a constant bulk speed of the CME during the spacecraft crossing. Then, we express the magnetic field profile as a function of spatial coordinates (B(x)) and apply the expansion correction. This allows us to plot B'(x'), where B' is the magnetic field, and

Wind NEAR 1997-12-10 $\Delta r = 0.18 \text{ au} / \Delta \alpha = 1.2^{\circ}$

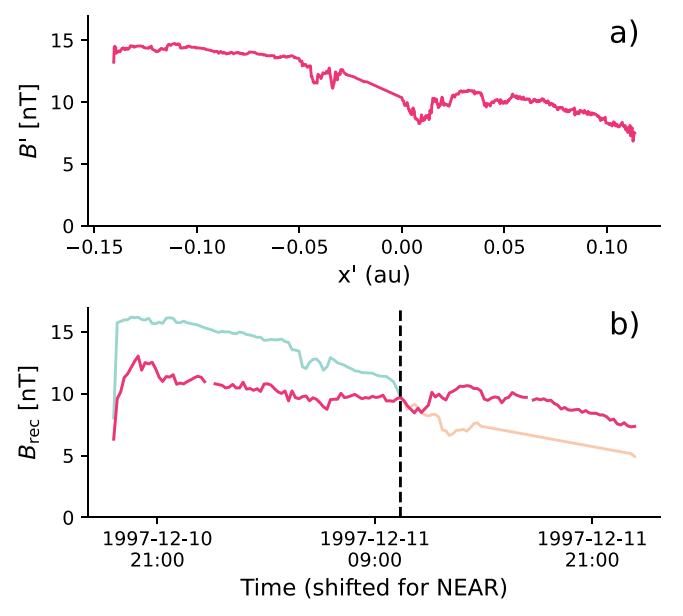


Figure 5. Panel (a) shows the instantaneous profile following the procedure of Démoulin et al. (2020) at Wind on 1997 December 10. Panel (b) shows the reconstructed profile for the Wind–NEAR event marked by a red line. Light green and orange lines correspond to the portions of the ME profile at Wind and NEAR that are not used to build the reconstructed profile. See Section 4.4 for more details.

x' is the spatial coordinates, both corrected for radial expansion. We follow this procedure at Wind, where solar wind plasma measurements are available. We find that the expansion-corrected front-to-back ratio following the procedure by Démoulin et al. (2020) is 1.7. This shows that most of the asymmetry measured at Wind (where the front-to-back ratio is 2.1) cannot be explained using the correction of Démoulin et al. (2020) alone that assumes self-similar expansion and no changes in the ME properties except for expansion. This result is consistent with the fact that this ME has a small local expansion with, however, large differences between Wind and NEAR in the magnetic field profiles.

Next, we compare the two "instantaneous" front-to-back ratios of the NEAR-Wind event: the one obtained by taking simultaneous measurements and the one obtained with the instantaneous profile following the procedure of Démoulin et al. (2020). We find a lower asymmetry with the simultaneous front-to-back ratio. This suggests, then, that the Démoulin et al. (2020) method does not capture all of the asymmetry by correcting for self-similar expansion deduced from the speed. This means that there must be significant aging of the ME that is independent of the expansion, or that the self-similar assumption does not hold. This agrees with the conclusion of Osherovich et al. (1993), who pointed out that both expansion and aging must contribute to the asymmetry of the magnetic field profile inside MEs.

4.4. Reconstruction of the "True" Magnetic Profile Inside MEs

We now use the simultaneous magnetic profiles of the same ME measured by two spacecraft to build a profile for which the temporal effects are reduced. We assume that, given the small angular separation, each spacecraft probes the same CME portion. Other than that, the reconstructed profile is built

relying purely on the data and without making any other assumptions, such as that of self-similarity or lack of aging beyond the changes due to radial expansion.

The reconstructed profile is built using the beginning of the measurements at the second spacecraft (SC2) and the end of the measurements at the first spacecraft (SC1). Such a profile should have its time dependency reduced compared to the profile obtained from a single spacecraft. We switch from the measurements of SC2 to those by SC1 as follows. We find the time closest to the center of the ME as measured by SC2 when the magnetic field strength measurements at SC1 and SC2 are equal. This ensures a continuous reconstructed profile. It is not guaranteed that SC1 and SC2 measure the same magnetic field strength at some point, but it is the case for the event highlighted here.

The result for the Wind-NEAR event is plotted in panel (b) of Figure 5. The red profile is the reconstructed profile, while the light green and orange profiles correspond to the original profiles as measured by SC1 and SC2, respectively. We point out that the reconstructed profile only takes the front part of the NEAR magnetic field ME profile and is thus not impacted by the linear interpolation of the back of the NEAR ME.

The front-to-back ratio for the reconstructed profile is 1.5 for the NEAR–Wind event. As a reminder, the front-to-back ratio from the spacecraft measurements for the Wind–NEAR event is 2.1 for both profiles. We thus find here that the reconstructed profile is more symmetric than the measured magnetic field profiles. A similar result is obtained with the DiP values. We find that the DiP is 0.48 for the reconstructed Wind–NEAR profile. This result is expected with the strong correlation previously found between the front-to-back ratio and DiP. The profile obtained from the Wind–NEAR event is then significantly flatter than that measured directly or as compared to the "instantaneous" profile following the procedure of Démoulin et al. (2020) for which the front-to-back ratio is 1.7.

As this reconstruction only reduces the time dependency of the measurements by half at most, it is possible that the true magnetic field profile of the ME (meaning a "cut" through the ME at a given time) seen by Wind and NEAR would be flat, which is extremely different from the CME profiles observed by each of the two spacecraft.

In spite of its simplicity, this method allows us to reduce the aging effect of the ME probed by Wind and NEAR, since the asymmetry is lower in both reconstructed profiles. However, this approach could be improved by adding geometrical constraints in order to find a more appropriate time to switch from one in situ profile to the other. Overall, the reduction of the ME magnetic field asymmetry results from partially correcting for the effect of aging (the time-dependent evolution of the ME, which differs from radial expansion), which has been reduced by performing such a reconstruction.

This technique can be applied when two spacecraft are radially aligned. The exact limit of the angular separation that the "simultaneous measurements" technique requires needs more cases to be firmly established. From the Wind–Juno case discussed in Section 3.1, it appears that a radial separation of 0.07 au and an angular separation of 6.6 (corresponding to an arc of 0.12 au) correspond to a case when spatial/angular variations dominate over aging. Moreover, CMEs can propagate up to 10° in an off-radial direction (Al-Haddad et al. 2022). Thus, any nonradial flows (even small) would

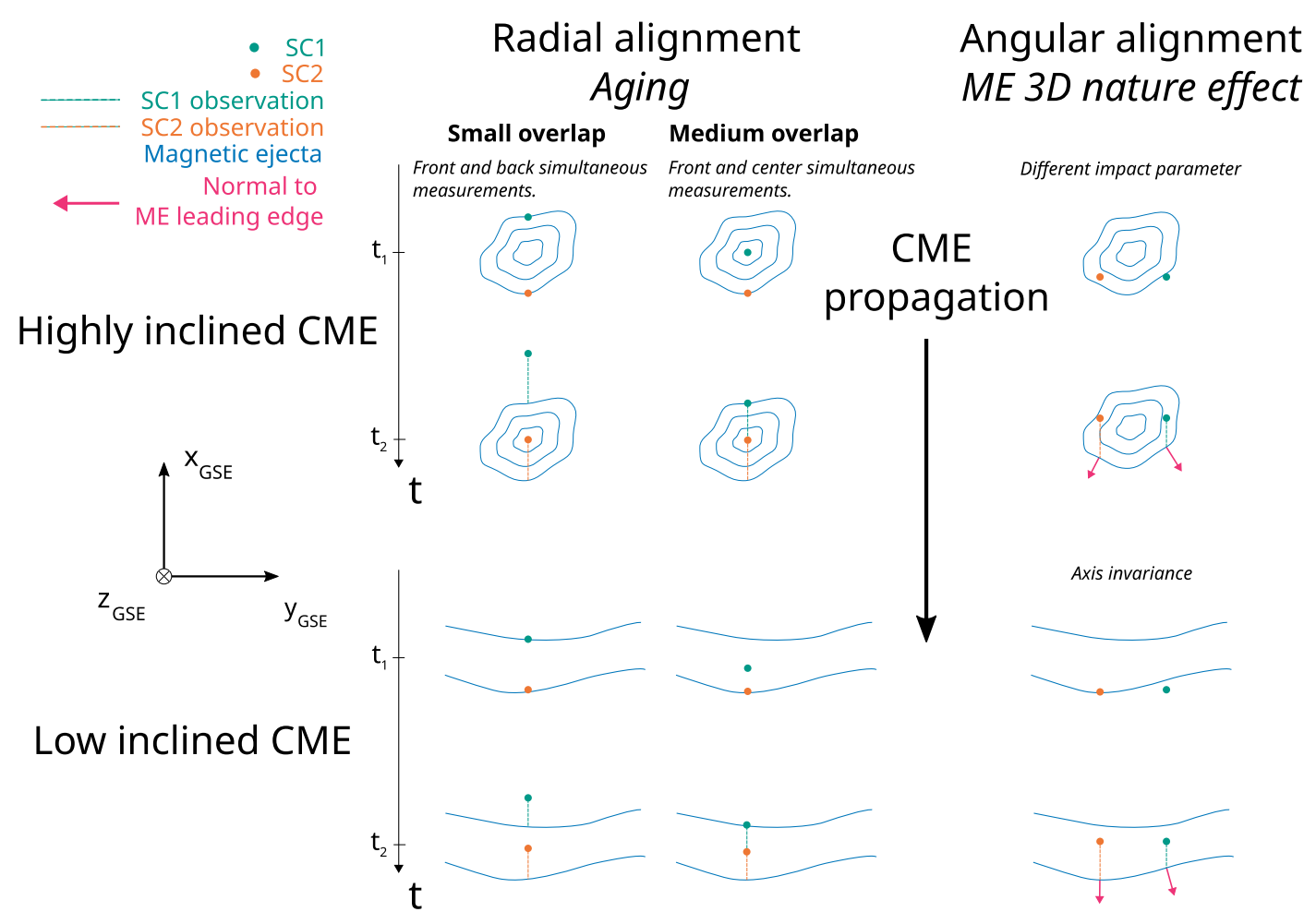


Figure 6. Schematic showing the different possible configurations of the spacecraft during a simultaneous measurement of a low and highly inclined ME.

change what we would define as a good "radial alignment." That said, even with a perfect radial alignment, the position of the spacecraft with respect to the bulk motion of the CME is still unknown and cannot be established using our limited measurements. This problem is further complicated by the presence of expansion and flows, radial and nonradial, inside the CME. A dedicated cluster of spacecraft that are radially and angularly aligned would provide measurements that will help disentangle those effects.

5. The Potential of Simultaneous Measurements

As shown with our two detailed case studies in Sections 3.1 and 4.1, simultaneous ME measurements by two spacecraft in close proximity can help us to better understand the ME structure and its spatial and temporal variations. Figure 6 shows a sketch highlighting the different possible configurations for an ME simultaneously measured by two spacecraft and discusses the different physical processes that can be studied with such configurations. The magnetic structure of the ME represented by the generalized cross section is in blue. The two spacecraft are in green and orange.

The left column of the figure shows the simultaneous measurement of an ME with radially aligned spacecraft for two different ME orientations. If the two spacecraft are separated approximately by the radial size of the ME (left column), simultaneous measurements of the front and back of the ME

can be obtained to investigate the asymmetry, but there is only limited overlapping time, i.e., during which both spacecraft are inside the ME. This approximately corresponds to the situation for the Wind-NEAR event shown in Figure 4.

If the radial separation between the two spacecraft is smaller than the size of the ME (middle column), both spacecraft are inside the ME at the same time for a longer period of time. The longer the overlap, the more the aging can be studied and the time dependency of the profile can be corrected. The configuration for the "medium overlap" (separation similar to the ME radial size) as presented in Figure 6 corresponds to the case where the time dependency can be, in theory, divided by 2.

The right column of Figure 6 shows the scenario when both spacecraft are at approximately the same heliocentric distance but have some angular separation. In this case, the simultaneous measurements can be used to study the ME 3D nature. In particular, we can test the assumption of axis invariance of the ME, which is a necessary assumption in fitting models (see discussion in Al-Haddad et al. 2019). The angular separation that would be optimal for this configuration is still unknown, but it is in the range of 2°–12° based on our results in this and previous studies. As highlighted by the Wind–Juno event (see Section 3.1), the two spacecraft in this configuration should be, as much as possible, at the same radial distance, so that propagation effects between the two spacecraft can be neglected.

6. Conclusions

In the present study, we analyze, for the first time, simultaneous measurements of MEs by two spacecraft at different radial distances to investigate the effect of the temporal evolution of the CME as it passes over a spacecraft (aging), as seen from the measured ME properties. We start from a database containing measurements of more than 2000 CMEs over 4 decades to obtain 19 multispacecraft simultaneous measurements as the core of the present study. We first compare ME properties probed by two spacecraft when they are close to each other, and then we focus on investigating the effect of aging on the ME magnetic field strength profile near 1 au.

Past statistical studies of CMEs measured at different distances indicate that the ME magnetic field strength decreases relatively steeply ($\propto r^{-\gamma}$ with $\gamma \sim 1.8$ –1.9; Gulisano et al. 2010; Winslow et al. 2015) with heliocentric distance up to about 1 au. Based on these studies, we would expect the magnetic field strength to decrease by 20%–40% between two spacecraft separated radially by 0.1–0.2 au. This is not what we find here for some events in our catalog.

One of the key findings of this work is that, in fact, for six out of 19 CMEs, the spacecraft further away from the Sun measures the stronger ME mean magnetic field strength. This may indicate that spatial variations or other phenomena within an ME may result in differences in magnetic field strength of at least 20%. Moreover, this catalog allows us to quantify the magnitude of the difference in the ME properties between two spacecraft that measure different parts of the CME at the same time. We find that the ME mean magnetic field varies by 1.3 nT, on average, and the DiP parameter varies by 0.04 between the two spacecraft. This is another key result of the study; it is an estimate of the variability of these parameters when measured by a single spacecraft. It corresponds to a relative difference between 14% and 18% for the mean magnetic fields when comparing, respectively, with the average of the most probable and median ME magnetic profile deduced in Regnault et al. (2020). Given the low number of CMEs in our sample, it is difficult to generalize these findings to all CMEs. However, these shed light on the potential of simultaneous measurements to extend our knowledge of CMEs, as discussed in Section 5.

Furthermore, we looked in detail at one specific event for which the two spacecraft (Wind and NEAR) had a very small angular separation and a radial separation similar to the ME radial size. We computed the simultaneous front-to-back ratio of the ME, taking advantage of this unique spacecraft configuration. We found that aging has a significant influence on the magnetic field strength profile of an ME measured by a single spacecraft. We then compared this measure with the "instantaneous" magnetic profile deduced using the Démoulin et al. (2020) methodology, which is purely based on selfsimilar expansion using the measured velocity profile. We found that the simultaneous front-to-back ratio is lower than the one computed using the "instantaneous" profile. This indicates that self-similar expansion is not the only cause of this aging. Results found in this study suggest that one should not to equate ME aging with expansion, as it is clear from this study that these two terms are not equivalent, at least in the case study we present.

Notable spatial variations of the ME properties on an angular extent of 8° have been reported by Hu et al. (2022) when using

a fitting technique with multiple in situ profiles inherent to the model of magnetic structure they used. Internal magnetic reconnection or interaction with the solar wind can locally change the ME properties and explain these differences. In addition, 3D variations within the ME may also contribute to these discrepancies, even for angular separations smaller than 10° , confirming conclusions reached with separations of $\sim\!0.5^{\circ}$ (Lugaz et al. 2018). However, such physical processes have not been well studied before, largely due to the lack of dedicated missions (we only found 19 such events over more than 4 decades of in situ measurements). Conversely, models also fail to accurately describe the ME structure when the angular separation is too large, as shown in Weiss et al. (2021).

Despite our efforts in gathering as many CMEs as possible, we are still limited to 19 events. This low number of events and the lack of readily available plasma measurements taken by spacecraft in our data set limits the extent and type of investigations that can be done at present. Nevertheless, as shown in this paper, simultaneous multispacecraft measurements within CMEs present valuable opportunities to better understand their magnetic structure. Obtaining more simultaneous multispacecraft plasma and magnetic field measurements with the Solar Orbiter, Parker Solar Probe, STEREO, and L1 assets with separations of 0.1–0.2 au, or a dedicated multispacecraft mission, should be a priority to understand the temporal and spatial variations within MEs, CMEs, and other solar wind structures.

Acknowledgments

All of the data have been retrieved using a python interface of the Coordinated Data Analysis System (CDAS) web service (https://pypi.org/project/cdasws/). The data sets used in this study are AC_H3_MFI (1 s resolution) and AC_HO_SWE (64 s resolution) for ACE, HELIOS1_40SEC_MAG-PLASMA and HELIOS2_40SEC_MAG-PLASMA for Helios-1/2 (40 s resolution), SOLO LL02 MAG (8 s resolution) and SOLO L2 SWA-PAS-GRND-MOM (4 s resolution) for Solar Orbiter, PSP_FLD_L2_MAG_RTN_1MIN (60 s resolution) and PSP_ SWP_SPC_L3I (28 s resolution) for Parker Solar Probe, STA_L2_MAGPLASMA_1M STB_L2_MAGPLASand MA_1M (60 s resolution) for STEREO-A/B, WI_H0_MFI (60 s resolution) and WI_H1_SWE (92 s resolution) for Wind, 18 15SEC MAG (15 s resolution) for IMP, and PIONEERVE-NUS_MERGED_SOLAR-WIND_10M (600 s resolution) for PVO, except for the Juno and NEAR spacecraft, for which we use the Planetary Data System (https://pds.nasa.gov/).

All authors acknowledge grant 80NSSC20K0431. F.R., N.A., and W.Y. acknowledge grants 80NSSC21K0463 and AGS1954983. N.L. and F.R. acknowledge grant 80NSSC20K0700. C.J.F. acknowledges support from grants 80NSSC21K0463 and Wind's grant 80NSSC19K1293. E.D. acknowledges NASA grant 80NSSC19K0914 and funding by the European Union (ERC, HELIO4CAST, 101042188). Views and opinions expressed are however those of the author(s) only and do not necessarily reflect those of the European Union or the European Research Council Executive Agency. Neither the European Union nor the granting authority can be held responsible for them.

ORCID iDs

F. Regnault https://orcid.org/0000-0002-4017-8415

N. Al-Haddad https://orcid.org/0000-0002-0973-2027

N. Lugaz https://orcid.org/0000-0002-1890-6156

```
C. J. Farrugia https://orcid.org/0000-0001-8780-0673 W. Yu https://orcid.org/0000-0002-2917-5993 E. E. Davies https://orcid.org/0000-0001-9992-8471 A. B. Galvin https://orcid.org/0000-0003-3752-5700 B. Zhuang https://orcid.org/0000-0002-5996-0693
```

References

```
Al-Haddad, N., Galvin, A. B., Lugaz, N., Farrugia, C. J., & Yu, W. 2022, ApJ,
   927, 68
Al-Haddad, N., Nieves-Chinchilla, T., Savani, N. P., et al. 2013, SoPh,
   284, 129
Al-Haddad, N., Poedts, S., Roussev, I., et al. 2019, ApJ, 870, 100
Al-Haddad, N., Roussev, I. I., Möstl, C., et al. 2011, ApJ, 738, L18
Bothmer, V., & Schwenn, R. 1998, AnGeo, 16, 1
Brueckner, G. E., Howard, R. A., Koomen, M. J., et al. 1995, SoPh, 162, 357
Burlaga, L., Sittler, E., Mariani, F., & Schwenn, R. 1981, JGR, 86, 6673
Burlaga, L. F. 1988, JGR, 93, 7217
Cane, H. V., Richardson, I. G., & Wibberenz, G. 1997, JGR, 102, 7075
Colin, L. 1980, JGR, 85, 7575
Davies, E. E., Forsyth, R. J., Good, S. W., & Kilpua, E. K. J. 2020, SoPh,
   295, 157
Davies, E. E., Forsyth, R. J., Winslow, R. M., Möstl, C., & Lugaz, N. 2021a,
    pJ, 923, 136
Davies, E. E., Möstl, C., Owens, M. J., et al. 2021b, A&A, 656, A2
Davies, E. E., Winslow, R. M., Scolini, C., et al. 2022, ApJ, 933, 127
Démoulin, P., Dasso, S., Lanabere, V., & Janvier, M. 2020, A&A, 639, A6
Eyles, C. J., Simnett, G. M., Cooke, M. P., et al. 2003, SoPh, 217, 319
Farrugia, C. J., Berdichevsky, D. B., Möstl, C., et al. 2011, JASTP, 73, 1254
Farrugia, C. J., Burlaga, L. F., Osherovich, V. A., et al. 1993, JGR, 98, 7621
Good, S. W., Kilpua, E. K. J., LaMoury, A. T., et al. 2019, JGRA, 124, 4960
Gosling, J. T. 1990, Physics of Magnetic Flux Ropes (Washington, DC:
   American Geophysical Union), 343
Gulisano, A. M., Démoulin, P., Dasso, S., Ruiz, M. E., & Marsch, E. 2010,
   A&A, 509, A39
Harrison, R. A., Davies, J. A., Rouillard, A. P., et al. 2009, SoPh, 256, 219
Howard, R. A., Moses, J. D., Vourlidas, A., et al. 2008, SSRv, 136, 67
Howard, T. A., & DeForest, C. E. 2012, ApJ, 746, 64
Hu, Q., & Sonnerup, B. U. Ö. 2002, JGRA, 107, 10
Hu, Q., He, W., & Chen, Y. 2022, FrP, 10, 960315
Janvier, M., Winslow, R. M., Good, S., et al. 2019, JGRA, 124, 812
Jian, L., Russell, C., Luhmann, J., & Skoug, R. 2008, AdSpR, 41, 259
```

```
Jian, L., Russell, C. T., Luhmann, J. G., & Skoug, R. M. 2006, SoPh, 239, 393
Kilpua, E., Jian, L., Li, Y., Luhmann, J., & Russell, C. 2011, JASTP, 73,
  1228
Klein, L. W., & Burlaga, L. F. 1982, JGR, 87, 613
Leitner, M., Farrugia, C. J., Möstl, C., et al. 2007, JGRA, 112, A06113
Lepping, R. P., Jones, J. A., & Burlaga, L. F. 1990, JGR, 95, 11957
Liu, Y., Richardson, J., & Belcher, J. 2005, P&SS, 53, 3
Lugaz, N., Farrugia, C. J., Smith, C. W., & Paulson, K. 2015, JGRA, 120, 2409
Lugaz, N., Farrugia, C. J., Winslow, R. M., et al. 2018, ApJ, 864, L7
Lugaz, N., Salman, T. M., Winslow, R. M., et al. 2020, ApJ, 899, 119
Lugaz, N., Salman, T. M., Zhuang, B., et al. 2022, ApJ, 929, 149
Lundquist, S. 1951, PhRv, 83, 307
Martinić, K., Dumbović, M., Temmer, M., Veronig, A., & Vršnak, B. 2022,
   A&A, 661, A155
Marubashi, K. 1986, AdSpR, 6, 335
Masías-Meza, J. J., Dasso, S., Démoulin, P., Rodriguez, L., & Janvier, M.
  2016, A&A, 592, A118
Möstl, C., Farrugia, C. J., Biernat, H. K., et al. 2009a, SoPh, 256, 427
Möstl, C., Farrugia, C. J., Miklenic, C., et al. 2009b, JGRA, 114, A04102
Möstl, C., Isavnin, A., Boakes, P. D., et al. 2017, SpWea, 15, 955
Möstl, C., Weiss, A. J., Bailey, R. L., et al. 2020, ApJ, 903, 92
Mulligan, T., Reinard, A. A., & Lynch, B. J. 2013, JGRA, 118, 1410
Mulligan, T., Russell, C. T., Anderson, B. J., et al. 1999, JGR, 104, 28217
Nakwacki, M. S., Dasso, S., Démoulin, P., Mandrini, C. H., & Gulisano, A. M.
  2011. A&A. 535. A52.
Nieves-Chinchilla, T., Vourlidas, A., Raymond, J. C., et al. 2018, SoPh,
Osherovich, V., Farrugia, C., & Burlaga, L. 1993, AdSpR, 13, 57
Owens, M. J., Lockwood, M., & Barnard, L. A. 2017, NatSR, 7, 4152
Regnault, F., Janvier, M., Démoulin, P., et al. 2020, JGRA, 125, e28150
Richardson, I. G. 2014, SoPh, 289, 3843
Richardson, I. G., & Cane, H. V. 2010, JGRA, 115, A07103
Riley, P., Linker, J., Lionello, R., et al. 2004, JASTP, 66, 1321
Salman, T. M., Lugaz, N., Farrugia, C. J., et al. 2020a, ApJ, 904, 177
Salman, T. M., Winslow, R. M., & Lugaz, N. 2020b, JGRA, 125,
  e2019JA027084
Tousey, R. 1973, BAAS, 5, 419
Vandas, M., & Romashets, E. P. 2003, A&A, 398, 801
Wang, C., Du, D., & Richardson, J. D. 2005, JGRA, 110, A10107
Weiss, A. J., Moestl, C., Davies, E. E., et al. 2021, A&A, 656, A13
Winslow, R. M., Lugaz, N., Philpott, L. C., et al. 2015, JGRA, 120, 6101
Winslow, R. M., Lugaz, N., Schwadron, N. A., et al. 2016, JGRA, 121, 6092
Winslow, R. M., Lugaz, N., Scolini, C., & Galvin, A. B. 2021, ApJ, 916, 94
```